An iterative algorithm for computing aeroacoustic integrals with application to the analysis of free shear flow noise

Florent Margnat, Véronique Fortuné

An iterative algorithm for computing aeroacoustic integrals with application to the analysis of free shear flow noise

Florent Margnat[a)]
DynFluid, Arts et Metiers ParisTech, 151 Boulevard de l'Hopital, 75013 Paris, France

Véronique Fortuné
Department of Fluid Flow, Heat Transfer and Combustion, Institute PPRIME, Université de Poitiers, ENSMA, CNRS, Bât. K, 40 Avenue du recteur Pineau, 86022 Poitiers Cedex, France

(Received 21 December 2009; revised 15 June 2010; accepted 18 June 2010)

An iterative algorithm is developed for the computation of aeroacoustic integrals in the time domain. It is specially designed for the generation of acoustic images, thus giving access to the wavefront pattern radiated by an unsteady flow when large size source fields are considered. It is based on an iterative selection of source-observer pairs involved in the radiation process at a given time-step. It is written as an advanced-time approach, allowing easy connection with flow simulation tools. Its efficiency is related to the fraction of an observer grid step that a sound-wave covers during one time step. Test computations were performed, showing the CPU-time to be 30 to 50 times smaller than with a classical non-iterative procedure. The algorithm is applied to compute the sound radiated by a spatially evolving mixing-layer flow: it is used to compute and visualize contributions to the acoustic field from the different terms obtained by a decomposition of the Lighthill source term. © *2010 Acoustical Society of America.* [DOI: 10.1121/1.3466986]

PACS number(s): 43.28.Ra, 43.20.Wd [AH] Pages: 1656–1667

I. INTRODUCTION

The computation of flow-generated noise has been the subject of a large number of studies[1,2] over the past 20 years, whose objective has been the reliable prediction of sound and the provision of insight regarding sound-production mechanisms. The direct acoustic computation by means of Direct Numerical Simulations (DNS) or Large Eddy Simulations (LES) has been pursued by a number of authors (see for instance[3–5] for the computation of jet noise). Direct noise computation requires high order schemes in order to capture the broad range of time and length scales associated with the physics of aerodynamically-generated sound, and specific boundary treatment in order to deal with the radiation of sound waves. The high cost of such numerical tools is limiting, and flow-generated acoustic fields are often predicted via a hybrid approach, using acoustic analogies[6,7] or wave extrapolation methods.[8,9]

In these approaches, the governing equations are rearranged in the form of an inhomogeneous wave equation where the right-hand side is interpreted as a source term. Such procedures allow the acoustic emission of unsteady flows to be obtained in two stages: first, the flow is simulated, computational effort is dedicated to correctly capturing the flow scales, giving access to source quantities (or to acoustic quantities on the control surface in the case of a wave extrapolation methods); then, these quantities are propagated into the acoustic field, attention now being focused on correctly capturing the dynamics of the acoustic waves. Thanks to such source modeling and propagation, we have access to the noise generated by flows simulated using Computational Fluid Dynamics (CFD) methods which are not necessarily designed to simulate (e.g., the incompressible computations) or propagate (e.g., highly dissipative schemes) acoustic waves. Finally, if source quantities can be stored, the acoustic computation becomes a post-treatment problem, and so it can be tested and optimized, independent of the flow computation. Also, the same acoustic tool can be applied to source data from different CFD tools.

In addition to their usefulness for noise prediction, acoustic analogies offer a theoretical interest for the investigation of the aerodynamic noise mechanisms, providing a description of how acoustic waves can be excited by the aerodynamic fluctuations. Using the source term expression, source regions can be identified in the flow, as done by Freund[5] with Lighthill's analogy. Similar attempts to understand sound production by means of acoustic analogies have also been made recently by Bodony and Lele[10] who evaluated internal competition between the constitutive components of the total Lighthill source term (in particular cancellations between the momentum and entropic terms were identified). For another example, the question of the physics of flow-induced cylinder noise has been addressed by Gloerfelt *et al.*[11] through an exploitation of Curle's formalism.[12]

In the present paper, the numerical implementation of a retarded-potential integral is addressed in the time-domain, with application to the analysis of sound production by free shear-flows. An optimized method is provided for the computation of the acoustic quantity on an observer grid in order to construct the acoustic field. An originality of the approach is the use of an iterative algorithm to determine the observer points to which source points radiate. This procedure is faster than a search procedure based on test condition scanning of

[a)]Author to whom correspondence should be addressed. Electronic mail: florent.margnat@paris.ensam.fr

 0001-4966/2010/128(4)/1656/12/$25.00

all the source-observer pairs. Only fixed source domains are considered, however moving domains may be treated using the technique presented hereafter. This optimization allows us to extend the application of the analysis methodology presented previously by Cabana *et al.*[13]—which requires the computation of the acoustic contribution from various subcomponents of the total Lighthill source—to flows involving large volumetric source-domains.

The paper is organized as follows: current issues associated with the construction of the acoustic field are described before the optimized algorithm is introduced. Then results of test simulations of the efficiency are presented, and an estimation is provided for the computational cost reduction which can be achieved. Finally, an application of the algorithm is presented through an analysis of the noise generated by a spatially evolving mixing layer flow.

II. IMPLEMENTING AEROACOUSTIC INTEGRALS: CURRENT ISSUES

For an observer position $\mathbf{x}$ and at time t_a, the integral solution to an acoustic-analogy problem can be written, considering a source quantity S to be integrated over a source domain $\mathcal{D}$, as

$$p_a(\mathbf{x},t_a)=\int_{\mathcal{D}} S\left(\mathbf{y},t_a-\frac{|\mathbf{x}-\mathbf{y}|}{c_0}\right)\frac{d\mathbf{y}}{|\mathbf{x}-\mathbf{y}|}, \tag{1}$$

where c_0 is the ambient sound speed and $\mathbf{y}$ is the source point. This is known as the retarded potential integral, since, unless the source is compact, the difference in propagation distance between two source points implies that their respective contributions must be collected at different emission times in order that they reach the observer point at the same time.

Formally, it can be viewed as the integral to be handled at computing, e.g., the solution of Lighthill's[14] or Howe's[15] equations in free-field, the volumic or surfacic terms appearing in Curle's analogy[12] or the general form provided by Ffowcs-Williams and Hawkings,[16] or wave extrapolations.

Such integration must be carried out carefully, because the source quantity is only known at discrete points and times; it is therefore necessary to interpolate the source field to obtain the values at the exact position and time imposed by the retarded potential integral. This issue, which is even more critical when moving sources are considered, has been addressed by Brentner.[17] Subsequent contributions have provided useful improvements, see for example Prieur and Rahier.[18] Note that implementations of the acoustic analogy in the frequency domain (solving the inhomogeneous Helmholtz equation) alleviate the need for solving the retarded time equation, interferences between different source points being taken into account through the phase contained in the Fourier transform of the source terms and Green's function. The drawback is that on-the-fly acoustic predictions are not possible then, so that complete time series of flow data must be stored and interrogated afterwards.

In the present paper, we address the case in which the acoustic quantity must be computed at several observer points in order to build acoustic fields or instantaneous images, or short movies if needed. This procedure allows us to study the entire acoustic field generated by an unsteady flow, rather than simply computing the acoustic signal at a given observer point. An optimized method is presented which precludes the need to store all of the distances $|\mathbf{x}-\mathbf{y}|$ during computation. Such storage can be computationally expensive since such a set will be 4-dimensional for an acoustic field issuing from a two-dimensional (2D) source (which can either be a surface source in a 3D problem or a volume source in a 3D problem), and even 5D for an acoustic field from a 3D source.

In the following, it is assumed that Nt_s datafiles of the source term S can be computed and sampled at Δt_s.

A. Basic integration method

The most straightforward procedure for computing the acoustic field at fixed observer time and position involves summing the contributions of the Ny_s fixed source elements by a loop

$$p_a(\mathbf{x},t_a)=\sum_{j}^{Ny_s} S\left(\mathbf{y}_j,t_a-\frac{|\mathbf{x}-\mathbf{y_j}|}{c_0}\right)\frac{\Delta V_{y_j}}{|\mathbf{x}-\mathbf{y_j}|}, \tag{2}$$

where ΔV_{y_j} is the elementary volume attached to the j^{th} source element located at $\mathbf{y_j}$. At each iteration, the value of the source term S at $\mathbf{y_j}$ has to be read from files of index k and $k+1$ given by

$$k\Delta t_s \le t_a-\frac{|\mathbf{x}-\mathbf{y_j}|}{c_0}<(k+1)\Delta t_s \tag{3}$$

in order to perform an interpolation at the retarded time. That *reception time* procedure is sketched in algorithm 1. It leads to $2Ny_s$ In/Out operations, for each observer time and position at which the acoustic field is computed. This can be very expensive. If there are Nx_o points and Nt_o times in the acoustic domain, that is if acoustic fields at several discrete times are to be built, one have to insert the loop on j inside loops on i and l in the following discrete equation:

$$p_a(\mathbf{x_i},t_a^l)=\frac{1}{4\pi}\sum_{j}^{Ny_s} S\left(\mathbf{y}_j,t_a^l-\frac{|\mathbf{x_i}-\mathbf{y_j}|}{c_0}\right)\frac{\Delta V_{y_j}}{|\mathbf{x_i}-\mathbf{y_j}|}, \tag{4}$$

where i and l are the observer point and time index, respectively.

Algorithm 1. Sketch of a reception time algorithm (instructions 1 and 9 are optional).

```
1: for all observer times (fix t_a^l) do
2:     for all observer points (fix x_i) do
3:         for all source points (fix y_j) do
4:             k=l-int(r_ij/c_0Δt_s)-1
5:             load S(k), S(k+1)
6:             interpolate, add to p_a(x_i,t_a^l)
7:         end for
8:     end for
9: end for
```

An interesting procedure, presented by Casalino[19] and Kessler and Wagner,[20] suggests looping over datafiles, index k, rather than over observer times, index l. As sketched in

algorithm 2, let two successive datafields be read, saved at $k\Delta t_s$ and $(k+1)\Delta t_s$. Inside this loop over k, a loop over the source points $\mathbf{y_j}$ is inserted. At the end of the latter, every source contribution at a retarded time between $k\Delta t_s$ and $(k+1)\Delta t_s$ required to compute the acoustic field has been accumulated in the integral. In other words, the set of 2 datafields has radiated all its useful content, and the files can be closed and will not need to be opened again. A sufficient condition for this is that source and observer points be both fixed.

At a given step (k,j) in the loop over the datafields and source points, the acoustic discrete time index l and the interpolation time $(k+\omega)\Delta t_s$ (with $0 \leq \omega < 1$) are required in order to radiate to the observer point $\mathbf{x_i}$; these are given by

$$l = k + 1 + \mathrm{int}\left(\frac{r_{ij}}{c_0 \Delta t_s}\right),$$
$$\omega = 1 - \left[\frac{r_{ij}}{c_0 \Delta t_s} - \mathrm{int}\left(\frac{r_{ij}}{c_0 \Delta t_s}\right)\right], \tag{5}$$

where $r_{ij} = |\mathbf{x_i} - \mathbf{y_j}|$. It has been assumed that the acoustic time is discretized in the same way as the source time so that t_a^l can be defined by $l\Delta t_s$.

Algorithm 2. Sketch of an emission time algorithm.

```
1: for all source times (fix k) do
2:     load S(k), S(k+1)
3:     for all source points (fix y_j) do
4:         for all observer points (fix x_i) do
5:             l=k+1+int(r_ij/c_0Δt_s)
6:             interpolate, add to p_a(x_i,t_a^l)
7:         end for
8:     end for
9: end for
```

When r_{ij} is exactly a multiple of $c_0\Delta t_s$, the interpolation can be avoided $(\omega=0)$, and, using the k^{th} source field contribution, the observer time index l reduces to $l=(k+r_{ij}/c_0\Delta t_s)$ while in practical numerical computing, this exception does not occur.

Such a procedure, which uses the emission time as reference is sometimes referred to as an advanced-time approach and it allows a single reading of the source data files. A significant reduction of computational costs can be achieved, though this reduction depends on the architecture of the numerical code. Moreover, the advanced-time approach allows the acoustic computation to be run in parallel with the source-flow simulation, source data-saving is thus avoided. This is of great interest when volume sources are considered, especially in 3D.

The two above algorithms correspond, respectively, to the terminology used by Brentner[17] for Retarded-Time Algorithm and Source-Time Dominant Algorithm. However, the cited reference provides three mathematical formulations of the solution in the case of moving source and observer, while the present paper deals with the implementation of spatial and temporal loops in the frame of the solution (2) and for fixed source and observer.

B. Discussion on the required optimization

When numerous source and observer points are involved, the triple loop on the source time index, the observer location index and the source location index must be optimized in order to prevent prohibitive computational cost. If 2D acoustic fields are required, of, say, (200×200) points generated by about (200×200) points in a 2D source domain, this leads to 1,600 million distances r_{ij}. Such a large quantity of points cannot reasonably be stored in an array variable; the situation is clearly worse when a 3D volume source is considered.

To compute the sum in Eq. (4), one needs, for each source field pair defined by k, for each source point defined by j, for each observer point defined by i, to compute the integer reception time step and the fractional emission time step using (5), to interpolate the source quantity at $t=(k+\omega)\Delta t_s$ and to accumulate the result in the integral. Since the integer reception time step is deduced from the source time index and the source-observer distance, the latter, if it cannot be stored, must be computed again at each source step for all source-observer pairs.

Moreover, every contribution reaching an observer before $t=k_{\min}\Delta t_s + r_{\max}/c_0$ or after $t=k_{\max}\Delta t_s + r_{\min}/c_0$ will lead to an incomplete acoustic field, that is to say, there will exist at least one observer point which lacks the contribution of at least one source point. $k_{\min}$ and $k_{\max}$ stand for the indices of the first and last available source fields respectively. $r_{\min}$ and $r_{\max}$ stand for the minimum and maximum distances r_{ij} among all [source-observer] pairs. Complete acoustic fields are thus available over that length of time only, defined by

$$T_c = (k_{\max} - k_{\min})\Delta t_s - \frac{r_{\max} - r_{\min}}{c_0} \tag{6}$$

Every $l(i,j,k)$ giving a reception time outside of these limits [see Eq. (5)] means that the corresponding k^{th} contribution of the j^{th} source point to the integral at the i^{th} observer point deals with an incomplete acoustic field. Thus, the computation of the source-observer distance and the reception time index is *a posteriori* of limited use at this source step. Furthermore, in practice, first and last known source fields ($k_{\min}$ and $k_{\max}$) are fixed by the user once the source flow is converged, and most often, only pictures or short movies are needed, so that T_c comes out significantly small with respect to $(k_{\max}-k_{\min})\Delta t_s$. This trend depends on the relative shapes of both the acoustic and observer domains, and on c_0. Finally, T_c results from a compromise between how far the acoustic domain stretches, how many source fields can be generated, and on how long the computation can run. Consequently, an important fraction of the $Nt_s \times Nx_o \times Ny_s$ computations of the reception time index is useless.

In fact, some discrete values of the reception time index should be fixed, corresponding to complete and desired acoustic fields. Let one be chosen in particular. Then, for each source field pair, the integral accumulation concerns [source-observer] pairs verifying (5) only. Since the source time index k is the increment, an optimization could consist in sorting pairs by sets of the same $\mathrm{int}(r_{ij}/c_0\Delta t_s)$, and performing the accumulation only for the adequate group at

each k. It supposes such sets to be known, and stored, but the situation considered here is when neither this storage, nor that of any type of geometrical sorting operation involving every [source-observer] pairs, are possible.

In this case, what is needed is a method to cover a set of the similar values of $\mathrm{int}(r_{ij}/c_0\Delta t_s)$ without knowing which source-observer index pairs (i,j) make up this set. Such a method is described in the following section; this is one of the main contributions of the present paper.

III. A RING-GUIDED PROCEDURE

A. Principle

Let the reception time index l be fixed such that

$$k_{\min}\Delta t_s + r_{\max}/c_0 \leq l\Delta t_s \leq k_{\max}\Delta t_s + r_{\min}/c_0,$$

meaning that all the required source contributions for this acoustic time are known. (If more than one acoustic field is desired, the loop on l must be performed for each successive source field pair k in order to respect the emission-time principle of a unique source field reading.) For a fixed k, the [source-observer] pairs involved in the accumulation process are such that, see (5)

$$\underbrace{(l-(k+1))c_0\Delta t_s}_{r_1} \leq r_{ij} < \underbrace{(l-k)c_0\Delta t_s}_{r_2}. \tag{7}$$

Thus, if the source point j is also fixed, its contribution radiates to observer points located within a circular strip, a ring, centered on $\mathbf{y_j}$ between the radii r_1 and r_2. It is possible to cover this set of observer points without having the source-observer distances stored: tracking a point in the vicinity of the ring, running a procedure which is able to move from an observer point to another *staying in the vicinity of the ring*, and test the source-observer condition (7) distance only at these observer points. This amounts to a recursive marching. Thus, a loop over the observer points is avoided, as sketched in algorithm 3.

Algorithm 3. Sketch of a ring-guided emission time algorithm (instructions 4 and 7 are optional).

```
1: for all source times (fix k) do
2:     load S(k), S(k+1)
3:     for all source points (fix y_j) do
4:         for all observer times (fix t_a^l) do
5:             find i: r_1 ≤ r_ij < r_2
6:             interpolate, add to p_a(x_i, t_a^l)
7:         end for
8:     end for
9: end for
```

In the case of a rectangular shaped acoustic domain with a uniform grid, such a procedure can be implemented by splitting the ring into 4 arcs with right angles from the main directions. Then, e. g. for the top right arc, we begin directly above the source point and outside the ring (*limits*), we then move down, testing the source-observer distance; once the *annular district* is reached, we move right to the next observer column and start again from outside. This marching is illustrated in Fig. 1. The scheme assumes that $\Delta x_o \geq c_0\Delta t_s$, where Δx_o is the observer grid step, but such a rule can be relaxed by choosing a further horizontal line as the new starting point of each step. It is worth noting that the observer grid step has no influence on the precision of the computed acoustic pressure, since there is no relation between the observer points (through numerical schemes, for instance). However, the observer grid affects the global CPU-time and the efficiency of the algorithm, and determines the resolution of the output image.

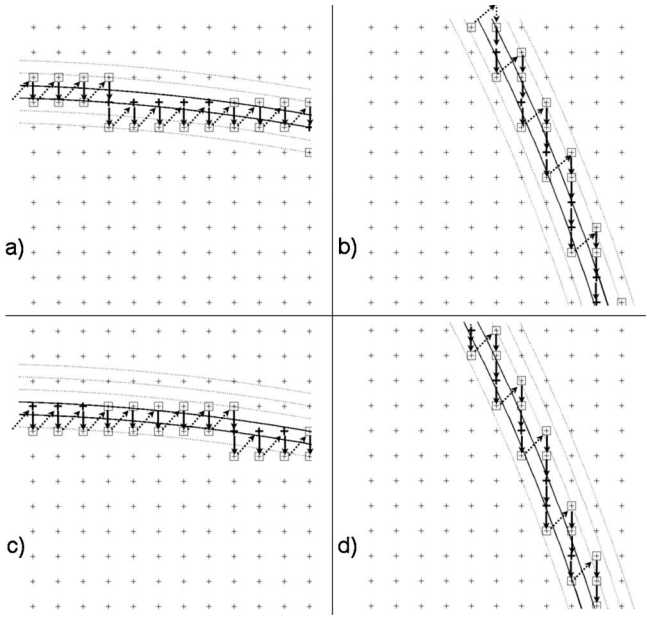

FIG. 1. Principle of the ring-guided procedure. Case $\Delta x_o = 2c_0\Delta t_s$. For one source time [(a) and (b)] and the following [(c) and (d)], at high emission angle [(a) and (c)] a low emission angle [(b) and (d)]. The procedure tracks observer grid points located between the two full-line circles (bold crosses) while minimizing the number of useless tested points (squares). The dotted-line circles correspond to other source times, and are plotted for visual aid.

The similarity with recursivity is strong, because the source observer distance computation and its comparison to the ring radii are performed only for observer points in the ring and for some of their neighbor. From a general point of view, the gain is achieved by guiding the search procedure along a narrow strip instead of scanning a complete two-dimensional area. Consequently, the problem lose one dimension and the CPU-time reduction is, in theory, of *the order of* $\sqrt{Nx_o}$.

B. Algorithm efficiency

In this section, the CPU-time reduction provided by the ring-guided procedure is estimated through test simulations in the configuration of Section IV. For all the test simulations, the extent of the source and observer domains are fixed. Their relative position and extent determine the acquisition time of the source fields. So the length of the datafile loop is fixed as well, $Nt_s = 755$. The test simulations ran on a Dual Core AMD Opteron Processor 280 at 2.4 GHz.

For the emission-time algorithm, see algorithm 2, one has to compute all the source-observer distances at each time step, and, for those corresponding to the current propagation time, to perform the interpolation and integration operations. The computation of the distance is far less demanding, but

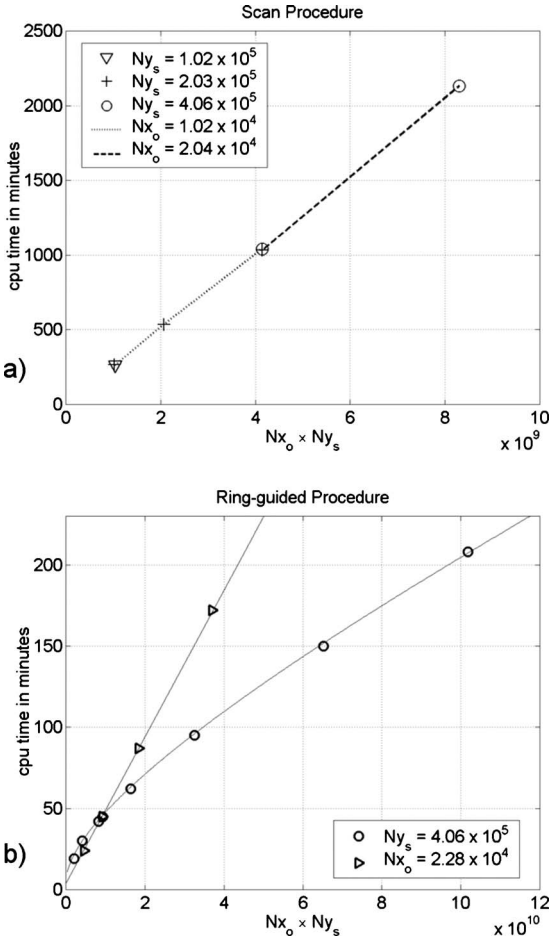

FIG. 2. CPU-time of test simulations with respect to the number of source-observer pairs, for different grid combination. (a) scanning emission-time procedure; (b) ring-guided emission-time procedure [solid line from estimation (9)].

the latter is performed only on a ring in the observer domain for each source point. Thus, finally, the CPU-time of this algorithm scales with the number of source-observer pairs, i.e., $Ny_s \times Nx_o$ multiplied by the number of data times Nt_s. This is illustrated in Fig. 2(a) for 5 combinations of the source and observer grids. The resulting linear regression function is

$$T_{SCAN} \propto 3.4 \;\; 10^{-10} \times Nt_s \times Nx_o \times Ny_s, \tag{8}$$

where T_{SCAN} is the CPU-time in minutes of a present simulation using the scanning emission time algorithm sketched in algorithm 2.

By avoiding numerous source-observer distance computations, the ring-guided algorithm, see algorithm 3, is much less time-consuming than the scanning one, as can be seen in Fig. 2(b). For example, the ratio is 35 for the case $Ny_s = 4.06 \;\; 10^5$ and $Nx_o = 1.02 \;\; 10^4$, and the ratio is 50 for the case $Ny_s = 4.06 \;\; 10^5$ and $Nx_o = 2.04 \;\; 10^4$. The ring-guided algorithm has also a different behavior with respect to the observer grid, however it is still proportional to the number of source points Ny_s. The relevant parameter concerning the observer grid is the ratio between the observer space step and the propagation distance during the source sampling time step, i.e., $\Delta x_o / c_0 \Delta t_s$. It is linked to Nx_o via the observer domain extent. The estimation of the cost associated with the ring-guided procedure is detailed in the Appendix, and can be written as

$$T_{RING} \propto \left(1.02 \frac{\Delta x_o}{c_0 \Delta t_s} + 0.92 \right) \;\; 10^{-9} \times Nx_o \times Ny_s, \tag{9}$$

where T_{RING} is the CPU-time in minutes of the simulation using the ring-guided emission time algorithm sketched in algorithm 3. Unlike T_{SCAN}, T_{RING} does not depend explicitly on Nt_s because it is determined by the total number of integration operations, which is always $Nx_o \times Ny_s$. However it may depend on changes in Δt_s. The present estimations are made for the generation of a single acoustic field image (i.e., at a single, given instant in time).

IV. APPLICATION TO THE ANALYSIS OF THE SOUND GENERATED BY A MIXING-LAYER

In this section, the procedure presented before for computing retarded-time integrals is applied to the analysis of sound radiated by a free shear flow. As a first application, we are interested here in the computation of the sound-field generated by vortex pairing in a two-dimensional mixing layer flow. This simple flow configuration was already used by previous authors[21–23] as a test case for studying sound production mechanisms in free shear flows. Our analysis methodology, based on a decomposition of the Lighthill source term, is first presented. Then a direct numerical simulation (DNS) of a 2D spatial mixing layer is performed, which provides source data for the acoustic computation. Finally, an analysis of the acoustic field radiated by the mixing layer is carried out, based on a comparison of the contributions from the source terms which appear in the decomposition.

A. Decomposition of the Lighthill source term

Cabana *et al.*[13] proposed a methodology, based on Lighthill's acoustic-analogy, aimed at providing physical insight regarding the mechanisms by which unsteady shear-flows generate sound. As Lighthill's source term comprises many physical effects which are not directly associated with sound production, the decomposition is proposed as a means of assessing the role played by the various pieces of the source term. The methodology, which allows us to 'look' inside the Lighthill source term in order to assess its content, is based on the following decomposition.

The classical expression of the Lighthill source term is considered, $S \approx \nabla \cdot \nabla \cdot (\rho \mathbf{uu})$, once entropic and viscous contributions have been neglected. This source term expression has been rewritten[13] with the velocity $\mathbf{u}$, vorticity $\boldsymbol{\omega}$, dilatation $\Theta = \nabla \cdot \mathbf{u}$ and density ρ fields appearing explicitly

$$\nabla\cdot\nabla\cdot(\rho\mathbf{uu}) = \underbrace{\rho\mathbf{u}\,\nabla\,\Theta}_{1} + \underbrace{\rho\Theta^2}_{2} + \underbrace{2\Theta\mathbf{u}\,\nabla\,\rho}_{3} + \underbrace{\rho\Delta\mathbf{u}^2/2}_{4}$$
$$+ \underbrace{\nabla\rho\,\nabla\,\mathbf{u}^2/2}_{5} + \underbrace{\rho\,\nabla\,\cdot\boldsymbol{\omega}\wedge\mathbf{u}}_{68} + \underbrace{\nabla\rho\cdot\boldsymbol{\omega}\wedge\mathbf{u}}_{7}$$
$$+ \underbrace{\mathbf{u}\cdot(\nabla\nabla\rho)\mathbf{u}}_{9} + \underbrace{\mathbf{u}\otimes\nabla\rho{:}\nabla\mathbf{u}}_{10}. \qquad (10)$$

In the present paper, the new subterm 68 is used to avoid redundancy in individual terms 6 and 8

$$\underbrace{\rho\,\nabla\,\cdot\boldsymbol{\omega}\wedge\mathbf{u}}_{68} = \underbrace{\rho\mathbf{u}\cdot\nabla\wedge\omega}_{6} - \underbrace{\rho\boldsymbol{\omega}\cdot\boldsymbol{\omega}}_{8}. \qquad (11)$$

Terms 1, 2 and 3 contain the dilatation and can be associated with acoustic phenomena. Terms 4 and 5 involve the kinetic energy, while terms 68 and 7 contain the Lamb vector, which are quantities identified in the theory of "vortex-sound" by Howe[15] and Powell.[24] Terms 9 and 10 are not easy to interpret. All terms, except 4 and 68, contains density fluctuations, through the density gradient or the dilatation, therefore they should vanish in simulation involving incompressible flow assumption. Source data issued from incompressible simulations are commonly used[25,26] in acoustic-analogy predictions, with reasonable success. So the "incompressible" terms 4 and 68 are expected to contain the main part of the sound production, and can be referred to as "driving terms." However their field may not be the same between the incompressible and compressible cases, because they contain the density field and, furthermore, because the velocity field does also contain compressible effects.

B. Flow computation

The compressible Navier-Stokes equations are solved[23] in a computational domain which includes both aerodynamic and acoustic fields of the flow. Such a calculation allows a direct computation of the sound production by the flow, and it allows us to obtain a large database of instantaneous flow quantities, which we can use for the evaluation of the acoustic-analogy source term. The direct computation of sound provides a reference solution for comparisons with results obtained from the acoustic analogy. A characteristic-based formulation[23,27] is used here, in order to facilitate the treatment of boundary conditions. Central sixth-order compact finite differences[28] are used to compute spatial derivatives, while time marching is performed by a fourth-order Runge-Kutta scheme.

The code is used to simulate the spatially evolving mixing-layer flow at $Re=\delta_\omega\Delta U/\nu=400$, where δ_ω is the initial vorticity thickness and $\Delta U=(U_h-U_l)$. The subscripts l and h refer to low and high speed flow, respectively. The initial mean streamwise velocity is given by a hyperbolic-tangent profile, and a small amplitude, incompressible disturbance field is added at the inflow boundary to initiate the transition process. The mixing layer is forced at its most unstable frequencies predicted by the linear theory,[29] in order to control the roll-up and vortex pairing process. A sponge zone is added to dissipate aerodynamic fluctuations before they reach the outflow boundary and to avoid any spurious reflection (see Ref. 23 for more details). The size of the computational domain is $Ly_1=800\times Ly_2=800$ which includes a large part of the acoustic field, and the grid resolution is $Ny_1=2071\times Ny_2=785$ with a stretched repartition in both directions. The subscripts 1 and 2 refer to the streamwise and transverse directions respectively.

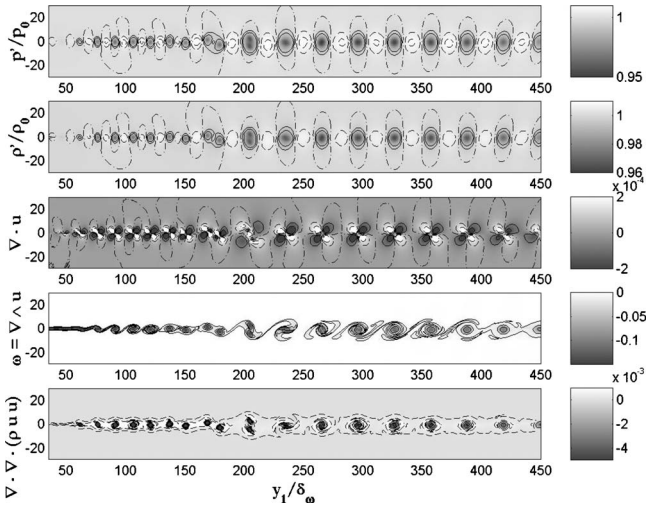

FIG. 3. Snapshots of the fluctuating pressure, density, dilatation, vorticity and Lighthill's source term (from top to bottom). The high speed flow $M=0.5$ is on top.

Snapshots of pressure, density, dilatation, vorticity are presented in Fig. 3, in the middle region of the computational domain. After the rolling up of the shear layer, vortex pairing occurs at a fixed position $y_1\approx 200\delta_w$ and period $T_p=80\delta_w/c_0$. The vortex signature in the dilatation field is a quadrupolar pattern. Density and pressure fields exhibit similar patterns, with successive low/high pressures at corresponding locations of high/low vorticity. The spatial evolution of the complete Lighthill source term (see last picture in Fig. 3) looks very similar to the vorticity field.

In order to quantify the competition between the subterms given by (10), a source term amplitude is defined as follows:

$$S_n = \frac{\max(T_n)-\min(T_n)}{\max(T_{Lighthill})-\min(T_{Lighthill})}, \qquad (12)$$

where T_n is the n^{th} source term, and min, max are the field extrema taken over the domain $(y_1/\delta_\omega=[100;300])\times(y_2/\delta_\omega=[-15;+15])$. The corresponding amplitudes are shown in Fig. 4. The "driving terms" ($\rho\Delta\mathbf{u}^2/2$ and $\rho\nabla\cdot\boldsymbol{\omega}\wedge\mathbf{u}$) dominate the others by two orders of magnitude. However, they may interfere destructively since, once combined, they have the same level as the the full Lighthill source term. Having said this, their sum is still 5 times greater than amplitude of term 9 (i.e., $\mathbf{u}\cdot(\nabla\nabla\rho)\mathbf{u}$) and about 60 times greater than that of term 1 ($\rho\mathbf{u}\nabla\Theta$), term 5 ($\nabla\rho\nabla\mathbf{u}^2/2$), term 7 ($\nabla\rho\cdot\boldsymbol{\omega}\wedge\mathbf{u}$) and term 10 ($\mathbf{u}\otimes\nabla\rho{:}\nabla\mathbf{u}$), while S_2 and S_3 (associated with $\rho\Theta^2$ and $2\Theta\mathbf{u}\nabla\rho$ respectively) seem negligible.

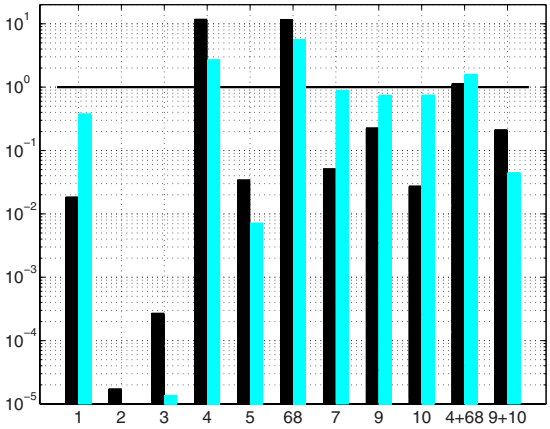

FIG. 4. (Color online) Respective amplitudes (black boxes) and acoustic powers (gray boxes) of the subterms of Eq. (10), in the source domain. The value $10^0=1$ corresponds to the full Lighthill source term.

C. Acoustic computation

From the simulation of the mixing layer flow, about 53 source fields are stored by pairing period during about $16T_p$. These large amount of data are necessary to provide a good precision of the retarded-time interpolation process and to perform the integration over the large source under consideration. The obtained database is the input of the following free-field solution of the Lighthill equation:

$$p_{a_n}(\mathbf{x},t)=\frac{1}{4\pi}\int_{\mathcal{D}} T_n\left(\mathbf{y},t_a-\frac{r}{c_0}\right)\frac{d\mathbf{y}}{r}, \tag{13}$$

where $r=|\mathbf{x}-\mathbf{y}|$. This solution is based on a free field Green's function for a uniform and quiescent medium. However, phenomena such as convection of acoustic waves or refraction by the shear flow are expected to be significant in the mixing-layer flow under consideration. As illustrated by Bogey *et al.*,[30] such convective effects can be taken into account through the integration of the Lighthill source quantity over a domain that contains the acoustic motion and the observer, provided that the source quantity is computed through a compressible simulation. According to this, the source domain $\mathcal{D}$ used in present approach is the whole computational domain $Ly_1\times Ly_2$ of the compressible simulation, in order to take into account the convective effects, which are included in the Lighthill source term.

The acoustic field is estimated on the same domain, on a square grid with $\Delta x_0=5.33$, which corresponds to 15 points per wavelength for the propagation at c_0 of a period T_p. Because the observer is included here in the source region, attention must be paid to the possible singularity of $1/r$. Here it is treated by removing a very small region close to the observer position from the source integration, as in other work.[31] Such a configuration contains $Ny_s\approx 1.6\times 10^6$ source points, $Nx_0\approx 2.3\times 10^4$ observer points, and $Nt_s\approx 755$ data files. So the estimated CPU-time using the scanning algorithm would be 6.5 days to build one acoustic full-field image of one source term. Since 9 source terms are considered, this requests to upgrade to the ring-guided algorithm. We have $\Delta x_0/(c_0\Delta t_s)\approx 3.5$, leading to $T_{RING}\approx 180$ min by subterm, given by Eq. (9).

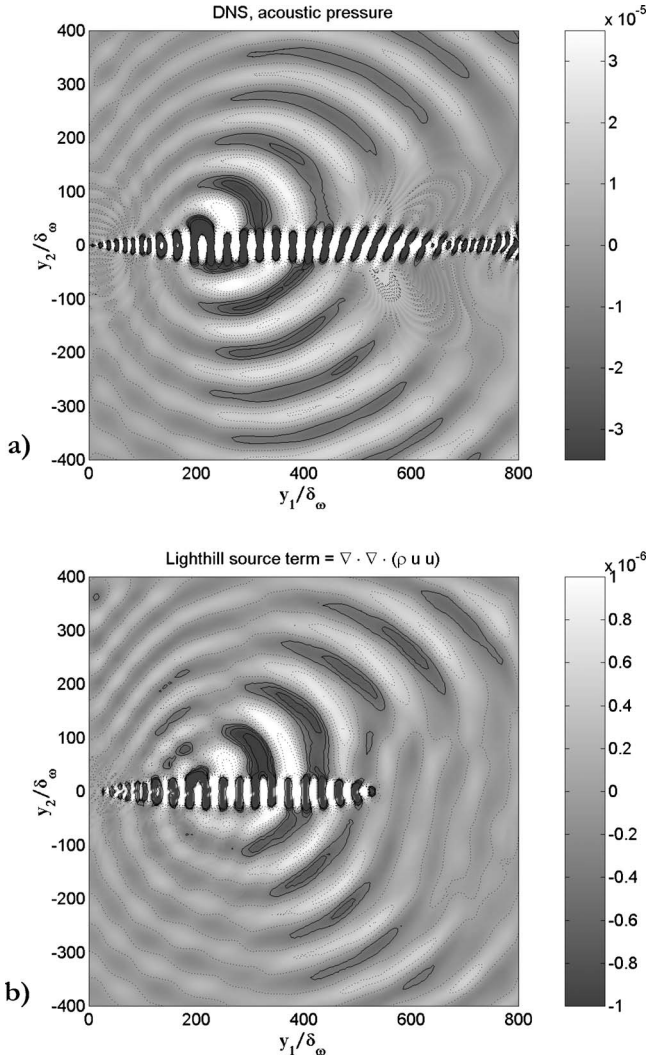

FIG. 5. Fluctuating pressure fields for a $Re=400$ mixing layer. (a) direct computation (reference solution); (b) result from Lighthill's analogy.

The interpolation procedure at $t_a=(k+\omega)\Delta t_s$ uses a Hermite method, the time derivative of the source term being also stored from the flow computation. As the truncation of the source field can lead to an erroneous acoustic computation,[32] a polynomial weighting is applied at the boundaries of the source domain.

As it can be seen in Fig. 5(a), the acoustic waves are generated in the pairing region, and the emission is mainly directed at 60 degrees from the flow axis in both sides of the flow. Radiation patterns provided by the acoustic analogy are in good qualitative agreement with the directly computed acoustic field, as shown in Fig. 5(b). A deviation in the wavefront pattern is mainly visible at 80 degrees above and under the flow axis. As the use of the 3D Green function instead of the 2D function involves differences in both amplitudes and phases, a quantitative agreement cannot be expected here. Indeed, the wave amplitude decreases with $1/r$ for a 3D propagation, while the 2D Green function decreases with $1/\sqrt{r}$ in the far-field. Radial profile of the acoustic pressure obtained from the analogy prediction and curves fitted with $1/r$ and $1/\sqrt{r}$ are provided in Fig. 6. The results from the analogy prediction follow well the $1/r$ decay, as expected.

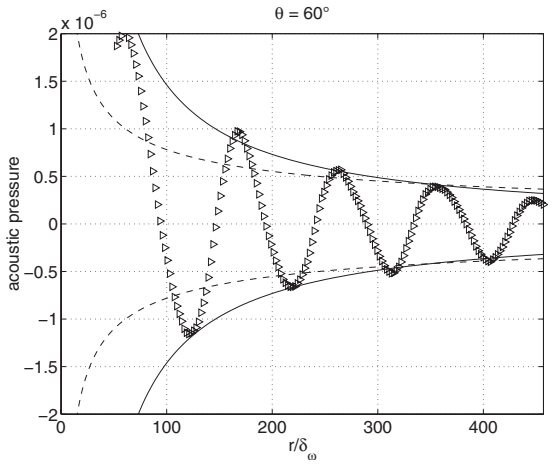

FIG. 6. Radial profile of acoustic pressure obtained from the acoustic analogy (symbols), source position $x_s=230\delta_\omega$, solid and dashed lines represent $1/r$ and $1/\sqrt{r}$ decay respectively.

This is an intrinsic limitation of the present analogy computation. In spite of this, meaningful information about the content of the Lighthill source term can be obtained through the comparison of the emission pattern radiated by the subterms of the decomposition (10) with respect to the resulting acoustic field.

D. Contributions of subterms to the sound field

In this section, we assess the radiation field computed using each of the subterms individually. While it is clear that it would not be physically meaningful to consider any of these sound fields alone, consideration of their contribution to the overall sound field can help shed light on their importance and physical meaning.

First, the acoustic power W_n radiated by the n^{th} source term given by (10) is estimated as the mean acoustic intensity vector flux

$$W_n = \frac{\int_\Sigma \int_0^{T_p} \frac{p_{a_n}^2(\mathbf{x},t)}{\rho_0 c_0} dt d\sigma_x}{\int_\Sigma \int_0^{T_p} \frac{p_{a_{Lighthill}}^2(\mathbf{x},t)}{\rho_0 c_0} dt d\sigma_x}, \tag{14}$$

where Σ is the circle of radius $300\delta_\omega$ centered on $(x_1,x_2)=(310\delta_\omega,0)$. This acoustic quantity is reported in Fig. 4. We observe that the dominant contributions are the "driving terms." But the contributions of term 1 ($\rho\mathbf{u}\nabla\Theta$), term 7 ($\nabla\rho\cdot\boldsymbol{\omega}\wedge\mathbf{u}$), term 9 ($\mathbf{u}\cdot(\nabla\nabla\rho)\mathbf{u}$) and term 10 ($\mathbf{u}\otimes\nabla\rho:\nabla\mathbf{u}$) seems also play a role in the overall acoustic field. The remaining terms have almost no contribution to the total emission.

As a departure point, we observe in Fig. 7(a) that the sound field resulting from the "driving terms" has no likeness with the acoustic field of the complete Lighthill source term which does not radiate downstream. The distinctive directional lobes, in particular, are not captured. The radiation pattern of the term 7 ($\nabla\rho\cdot\boldsymbol{\omega}\wedge\mathbf{u}$, not shown) is overall similar to the radiation of the "driving terms," but with a phase shift. Consequently, as it can be seen in Fig. 7(b), that radiation along the flow axis is almost cancelled when the acoustic patterns produced by each terms 4, 68 and 7 ($\rho\Delta\mathbf{u}^2/2$, $\rho\nabla\cdot\boldsymbol{\omega}\wedge\mathbf{u}$ and $\nabla\rho\cdot\boldsymbol{\omega}\wedge\mathbf{u}$ respectively) are combined.

We note however that the complete form of the distinct directive lobes are not fully reproduced, even if the contribution of the subterm 5 ($\nabla\rho\nabla\mathbf{u}^2/2$) is added [see Fig. 7(c)] to the radiated field. This is an interesting result because it is specific to the spatially evolving mixing layer. In the temporally evolving mixing layer, Cabana *et al.*[13] found that the total emission is recovered by the "driving terms" (4+68, i.e., $\rho\Delta\mathbf{u}^2/2+\rho\nabla\cdot\boldsymbol{\omega}\wedge\mathbf{u}$) combined with their compressible counterparts (5+7, i.e., $\nabla\rho\nabla\mathbf{u}^2/2+\nabla\rho\cdot\boldsymbol{\omega}\wedge\mathbf{u}$). In the spatially evolving mixing layer, if only the contributions of the same subterms are taken into account, some part of the total acoustic field is not captured. Additional terms are required to reproduce the correct radiation. Consequently attention is now turned to the remaining subterms.

Figures 7(d) and 7(e) show the acoustic field computed using term 1 ($\rho\mathbf{u}\nabla\Theta$), and using the sum of terms 1+4+5+68+7 (i.e., $\rho\mathbf{u}\nabla\Theta+\rho\Delta\mathbf{u}^2/2+\nabla\rho\nabla\mathbf{u}^2/2+\rho\nabla\cdot\boldsymbol{\omega}\wedge\mathbf{u}+\nabla\rho\cdot\boldsymbol{\omega}\wedge\mathbf{u}$) respectively. We see that the latter correctly reproduces the overall sound field (see Fig. 5 for comparison). In particular the characteristic directive lobes are well reproduced when the contribution of $\rho\mathbf{u}\nabla\Theta$ is included in the analogy prediction. So it is shown here that the term 1 ($\rho\mathbf{u}\nabla\Theta$), which was not important in the temporal mixing layer, is here instrumental, although it is very weak in the source domain. Being the product of the momentum vector by the dilatation gradient, it can be viewed as an acoustic transport term, and accounts for sound-flow interactions which are contained in the Lighthill source term.

The subterms 2 and 3 ($\rho\Theta^2$ and $2\Theta\mathbf{u}\nabla\rho$ respectively) were already shown (see Fig. 4) to have negligible contributions to the radiated field. Additionally, a strong cancellation arises between the contributions of the subterms 9 and 10 ($\mathbf{u}\cdot(\nabla\nabla\rho)\mathbf{u}$ and $\mathbf{u}\otimes\nabla\rho:\nabla\mathbf{u}$) and as it can be thus expected, the contribution of these terms is unimportant in the sound production (see Fig. 7(f)].

V. CONCLUSIONS

An optimized method has been developed for the computation of retarded-time integrals. It is presented using an algorithmic formalism, describing how the loops involved are organized, in order to show its advantage with respect to other more intuitive algorithms. The first and second algorithms introduced in algorithms 1 and 2, respectively, may be useful in the case of small quantities of source data and few observer locations, while the present optimization concerns the evaluation of the acoustic field on an observer grid, thus involving a large number of source-observer distances which cannot be stored in a local variable.

An iterative ring-guided procedure is proposed (see algorithm 3 and Fig. 1) which recursively searches observer points where the contribution of a given source point must be added once both the emission and reception time are fixed. Such a procedure appeared about 40 times faster than the second algorithm, in the simulations tested here. It still has not been developed for moving sources or observers, but it

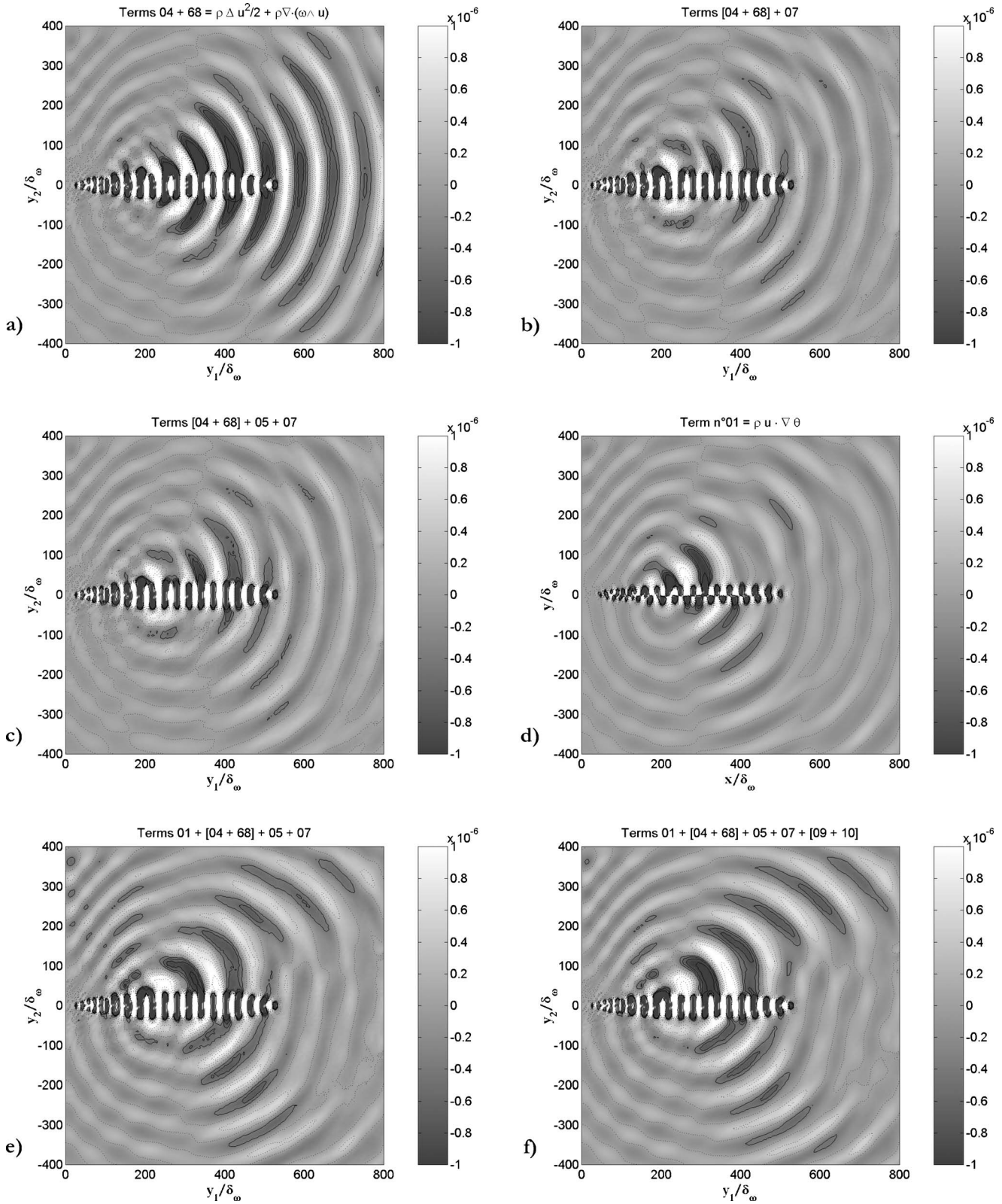

FIG. 7. Fluctuating pressure fields resulting from (a) summed contributions of driving source subterms (68+4), (b) summed contributions of subterms (68 +4) and 7, (c) summed contributions of subterms (68+4) and subterms 5 and 7. (d) the subterm 1 alone; (e) summed contributions of subterms 1+4+5 +68+7, (f) summed contributions of subterms 1+4+5+68+7+9+10.

can be used for all kinds of retarded-time integrals, such as volume sources in Lighthill-like formalisms as well as surface sources in Kirchhoff-like wave extrapolation methods. It keeps the advanced time principle allowing an acoustic prediction parallel to the flow simulation and an easy connection with usual CFD tools.

The CPU-time reduction obtained with this algorithm allows the application of an analysis methodology based on a Lighthill source term decomposition, for the study of sound production by a spatially evolving mixing-layer. The acoustic *field-image* of each subterm of the decomposition was computed while the number of source elements is relatively

large. Each contribution was compared with the radiation of the complete Lighthill source term, considering both the acoustic power and the orientation of the wavefronts which can be visualized in the acoustic fields. The latter showed two interesting physical results: first, the noise generated by the mixing-layer is the result of a balance between the incompressible "driving terms" based on vorticity and kinetic energy and their compressible counterparts, which generate sound cancellation downstream the pairing region; second, the acoustic pattern is strongly influenced by the subterm $\rho \mathbf{u} \nabla \Theta$. This fact is noteworthy since this term has no significant contribution in the case of a temporally evolving mixing-layer flow.[13] In the present spatially evolving flow, sound-flow interactions included in the Lighthill source can be responsible for the significant role played by this acoustic transport term.

ACKNOWLEDGMENTS

The algorithm development was supported by the French National Research Agency (ANR) via the 'BruitAero' program (Grant No. 05-BLAN-0208). Both authors thank Dr. P. Jordan for helpful discussions and for valuable advice in English language.

APPENDIX: EVALUATION OF THE RING-GUIDED PROCEDURE COST

Hereafter, the detail of the estimation given by (9) is provided. The analytical derivation is a difficult task while it will exhibit numerous cases depending on how the source and observer grids are staggered. However, it is possible to extract the general idea of the procedure in the present application without loss of generality.

1. Single source point

First, the output of the procedure is studied in the case of a single source point radiating in a quarter-plan of the observer domain. For one source point, the simulation is run in time, meaning that, as k is increasing, circles of decreasing radius, centered on the source, are scanned (see Fig. 1 and Section III A for the definition of r_1 and r_2), and the number of observer points is counted for each ring or time-step. The result is plotted in Fig. 8(a) for $\beta=\Delta x_o/c_0\Delta t_s=4$. The number of points found either inside or outside the ring by the procedure, is reported. The total number of points tested by the procedure is also plotted.

By construction of the procedure, as soon as it gets into the *annular region*, it moves to the next observer coordinate (see Fig. 1). Thus, whatever β, the number of points located inside is equal to the number of observer steps contained in this radius, that is $r_1/\Delta x_o$. It is observed that the total number of tested points is a linear function of $r_1/\Delta x_o$, with a coefficient of about 3.1 which does not depend on β. Though little dispersion is noted due to the discrete character of the topology, the evolution of the number of points located on the ring, or outside it, is also linear. The coefficients depend on the value of β, however. They are plotted in Fig. 8(b). Large values of β mean the thickness of the ring is small with respect to the observer grid step (see Fig. 1). Consequently,

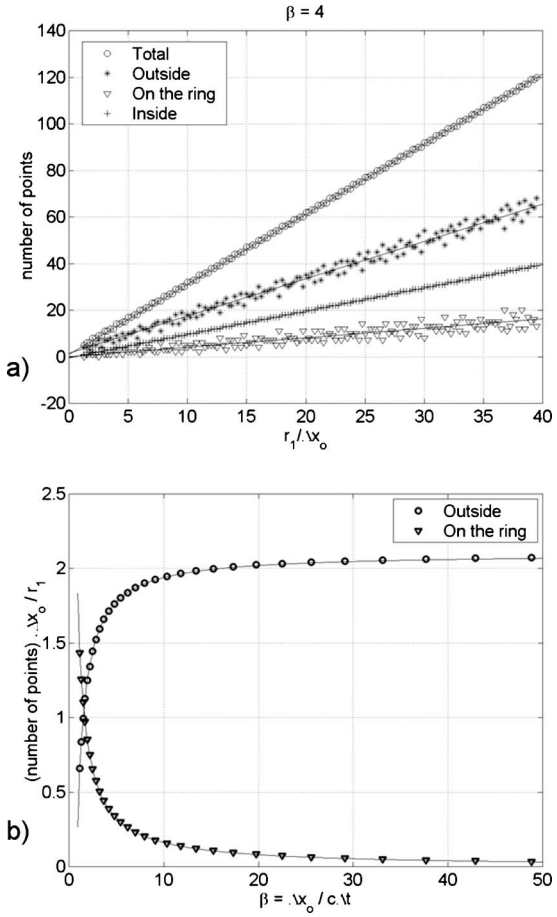

FIG. 8. Single source point test case. (a) Account of observer points concerned by the procedure marching as a function of the ring radius ($\beta=\Delta x_o/c_0\Delta t_s=4$). (b) Dependency on β of proportionality ratios between the number of points located on the ring, or outside it, and the ring radius $r_1/\Delta x_o$.

the probability of finding a point on the ring is small, and the fraction of tested points located outside is high.

Provided the whole quarter-ring is contained by the observer domain, the trends and the linear coefficients reported above do not depend on the exact location of the source point inside the observer grid. With this single source point case, it is shown how the CPU-time will be linked to β: if β is small, there is less waste in testing observer points located outside the ring.

The parameter β can also be viewed as the ratio of the number of time steps by source period to the number of observer grid steps by the corresponding acoustic wavelength. For example, at a given frequency, if the corresponding source period is described by around 100 time steps, and if the corresponding wavelength is described by around 10 listener points, the resulting value of β will be around 10, assuming a low subsonic flow (i.e., same sound speed in all directions).

2. Real source and observer domains

The single source case with only whole quarter-rings does not take into account that, in a real prediction, the rings can be truncated at the boundaries. This happens for large radii, or when the source point is located close to a boundary.

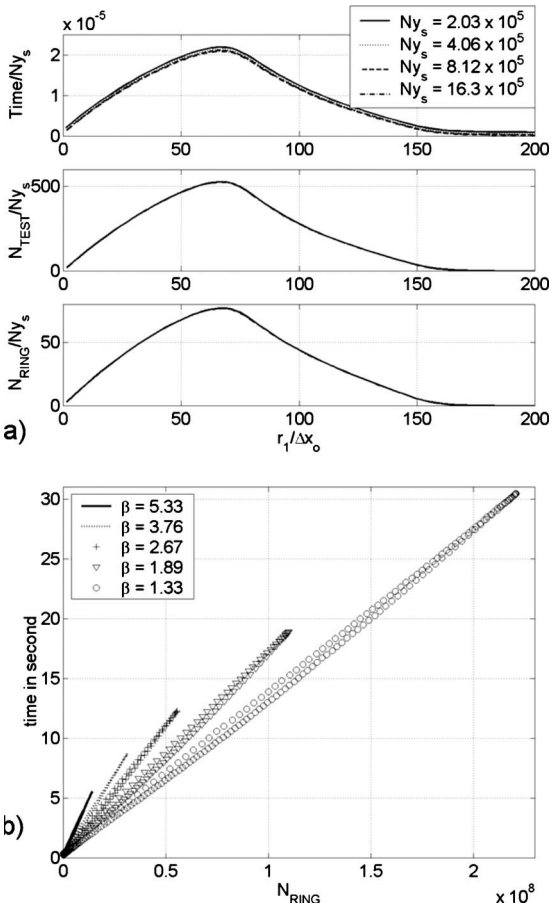

FIG. 9. (a) CPU-time and accounts of observer points concerned by the procedure marching as a function of the ring radius, for real source and observer domains, with different source grids. (b) CPU-time by ring step as a function of the number of [source-observer] pairs of which distance is between r_1 and r_2. Each symbol corresponds to a source file time step, that is an entire value of $|\mathbf{x}-\mathbf{y}|/c_0\Delta t_s$.

However, $N_{RING}(r_1)$ can be defined as the summation on every source point of the observer points enclosed by the ring, or truncated ring, centered on this source point and for a given interior radius r_1. $N_{TEST}(r_1)$ is defined as the total number of tested points for this radius—timestep. With these definitions, it can be seen in Fig. 9(a), for every r_1 involved in the test configuration described in Section IV C, that the number of tested points remains proportional to the number of points on the ring. (The shape of the curves are explained as follows: for high radii, only pairs having these extreme distances are involved and the rings are highly truncated, thus N_{RING} is small; for low radii, almost all the source terms radiate on whole rings, but then, the number of observer points in a ring is low because it is proportional to the radius, as for the single source point case).

Also, the CPU-time required by a time—or radius—step is proportional to these numbers. Finally, no dependency is noted of the proportionality ratios on source grid refinement. However, the ratios depend on β, as visible in Fig. 9(b) where CPU-time per time—radius—step is plotted as a function of N_{RING} for five observer grids and a given source grid.

Figure 9(b) suggests there exists a such as:

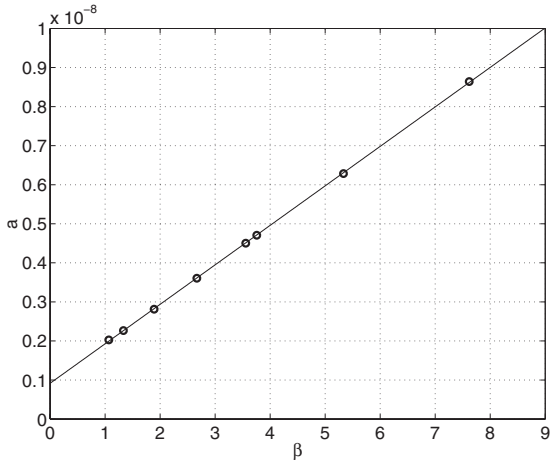

FIG. 10. Evolution of coefficient a with β. Symbols: different observer grids for $Ny_s=4.06\times10^5$; straight line: linear regression.

$$T(k) = a(\beta) \times N_{RING}(k),$$

where $T(k)$ is the CPU-time in minutes demanded by the k^{th} radius step. Consequently, the total time of the prediction will be given by:

$$T_{RING} = \sum_{k=1}^{Nt_s} T(k) = a(\beta) \times Nx_o \times Ny_s.$$

Indeed, the prediction of an acoustic field-image requires the collection, at each observer point, of the contribution of all the source points. A given source point radiates only once in time at a given observer point. That is why the summation of the N_{RING} always results in $Nx_o \times Ny_s$.

For all the test cases made at $Ny_s=4.06\times10^5$, the coefficient a is plotted in Fig. 10 as a function of β, and exhibits a linear dependence. The regression procedure provides the coefficients given in formula (9).

[1]T. Colonius and S. K. Lele, "Computational aeroacoustics: Progress on nonlinear problems of sound generation," Prog. Aerosp. Sci. **40**, 345–416 (2004).
[2]M. Wang, J. B. Freund, and S. K. Lele, "Computational prediction of flow-generated sound," Annu. Rev. Fluid Mech. **38**, 483–512 (2006).
[3]D. J. Bodony and S. K. Lele, "On using large-eddy simulation for the prediction of noise from cold and heated turbulent jets," Phys. Fluids **17**, 085103 (2005).
[4]C. Bogey and C. Bailly, "Investigation of downstream and sideline subsonic jet noise using large eddy simulation," Theor. Comput. Fluid Dyn. **20**, 23–40 (2006).
[5]J. B. Freund, "Noise sources in a low-Reynolds number turbulent jet at Mach 0.9," J. Fluid Mech. **438**, 277–305 (2001).
[6]B. Greschner, F. Thiele, A. Gurr, D. Casalino, and M. C. Jacob, "Prediction of sound generated by a rod airfoil configuration using a cubic explicit algebraic stress model for detached eddy simulation and the generalised lighthill/FW-H analogy, in 12th AIAA/CEAS Aeroacoustics Conference, Cambridge, MA (2006), AIAA Paper No. 2006-2628.
[7]E. Gröschel, W. Schröder, P. Renze, M. Meinke, and P. Comte, "Noise prediction for a turbulent jet using different hybrid methods," Comput. Fluids **37**, 414–426 (2008).
[8]N. Andersson, L. E. Eriksson, and L. Davidson, "Investigation of an isothermal Mach 0.75 jet and its radiated sound using large-eddy simulation and Kirchhoff surface integration," Int. J. Heat Fluid Flow **26**, 393–410 (2005).
[9]J. B. Freund, S. K. Lele, and P. Moin, "Calculation of the radiated sound field using an open Kirchhoff surface," AIAA J. **34**, 909–916 (1996).
[10]D. J. Bodony and S. K. Lele, "Low-frequency sound sources in high-speed turbulent jets," J. Fluid Mech. **617**, 231–253 (2008).

[11]X. Gloerfelt, F. Pérot, C. Bailly, and D. Juvé, "Flow-induced cylinder noise formulated as diffraction problem for low Mach number flows," J. Sound Vib. **287**, 129–151 (2005).
[12]N. Curle, "The influence of solid boundaries upon aerodynamic sound," Proc. R. Soc. London, Ser. A **231**, 505–514 (1955).
[13]M. Cabana, V. Fortuné, and P. Jordan, "Identifying the radiating core of Lighthill's source term," Theor. Comput. Fluid Dyn. **22**, 87–106 (2008).
[14]M. J. Lighthill, "On sound generated aerodynamically. I. General theory," Proc. R. Soc. London, Ser. A **223**, 1–32 (1952).
[15]M. S. Howe, "Contributions to the theory of aerodynamic sound, with applications to excess jet noise and the theory of the flute," J. Fluid Mech. **71**, 625–673 (1975).
[16]J. E. Ffowcs Williams and D. L. Hawkings, "Sound generated by turbulence and surfaces in arbitrary motion," Philos. Trans. R. Soc. London, Ser. A **264**, 321–342 (1969).
[17]K. S. Brentner, "Numerical algorithms for acoustic integrals: The devil is in the details," in 2nd AIAA/CEAS Aeroacoustics Conference, State College, PA (1996), AIAA Paper No. 96-1706.
[18]J. Prieur and G. Rahier, "Aeroacoustic integral methods, formulation and efficient numerical implementation," Aerosp. Sci. Technol. **5**, 457–468 (2001).
[19]D. Casalino, "An advanced time approach for acoustic analogy predictions," J. Sound Vib. **261**, 583–612 (2003).
[20]M. Kessler and S. Wagner, "Source-time dominant aeroacoustics," Comput. Fluids **33**, 791–800 (2004).
[21]T. Colonius, S. K. Lele, and P. Moin, "Sound generation in a mixing layer," J. Fluid Mech. **330**, 375–409 (1997).
[22]C. Bogey, C. Bailly, and D. Juvé, "Numerical simulation of sound generated by vortex pairing in a mixing layer," AIAA J. **38**, 2210–2218 (2000).
[23]C. Moser, E. Lamballais, and Y. Gervais, "Direct computation of the sound generated by isothermal and non-isothermal mixing layers," in 12th AIAA/CEAS Aeroacoustics Conference, State College, PA (2006), AIAA Paper No. 2006-2447.
[24]A. Powell, "Theory of vortex sound," J. Acoust. Soc. Am. **36**, 177–195 (1964).
[25]J. B. Boersma, "Large eddy simulation of the sound field of a round jet," Theor. Comput. Fluid Dyn. **19**, 161–170 (2005).
[26]F. Golanski, V. Fortuné, and E. Lamballais, "Noise radiated by a non-isothermal temporal, mixing layer. Part II: Prediction using DNS in the framework of low Mach number approximation," Theor. Comput. Fluid Dyn. **19**, 391–416 (2005).
[27]J. Sesterhenn, "A characteristic-type formulation of the Navier-Stokes equations for high order upwind schemes," Comput. Fluids **30**, 37–67 (2000).
[28]S. K. Lele, "Compact finite difference schemes with spectral like resolution," J. Comput. Phys. **103**, 16–42 (1992).
[29]A. Michalke, "On spatially growing disturbances in an inviscid shear layer," J. Fluid Mech. **23**, 521–544 (1965).
[30]C. Bogey, X. Gloerfelt, and C. Bailly, "An illustration of the inclusion of sound-flow interactions in Lighthill's equation," AIAA J. **41**, 1604–1606 (2003).
[31]C. Schram, "A boundary element extension of Curle's analogy for non-compact geometries at low-Mach numbers," J. Sound Vib. **322**, 264–281 (2009).
[32]P. Martínez-Lera and C. Schram, "Correction techniques for the truncation of source field in acoustic analogies," J. Acoust. Soc. Am. **124**, 3421–3429 (2008).